JACS
JOURNAL OF THE AMERICAN CHEMICAL SOCIETY

Subscriber access provided by American Chemical Society

Article

Polyynes as a Model for Carbyne: Synthesis, Physical Properties, and Nonlinear Optical Response

Sara Eisler, Aaron D. Slepkov, Erin Elliott, Thanh Luu,
Robert McDonald, Frank A. Hegmann, and Rik R. Tykwinski

J. Am. Chem. Soc., **2005**, 127 (8), 2666-2676• DOI: 10.1021/ja044526l • Publication Date (Web): 03 February 2005

Downloaded from http://pubs.acs.org on March 24, 2009

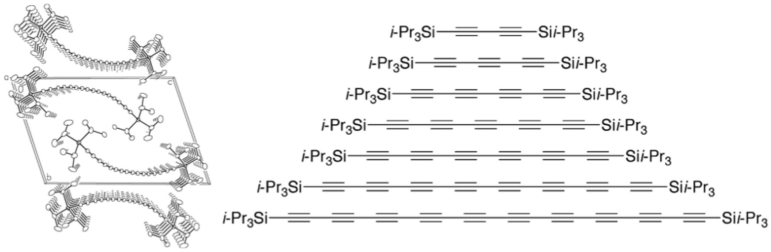

More About This Article

Additional resources and features associated with this article are available within the HTML version:

- Supporting Information
- Links to the 29 articles that cite this article, as of the time of this article download
- Access to high resolution figures
- Links to articles and content related to this article
- Copyright permission to reproduce figures and/or text from this article

View the Full Text HTML

ACS Publications
High quality. High impact.

Journal of the American Chemical Society is published by the American Chemical Society. 1155 Sixteenth Street N.W., Washington, DC 20036

J|A|C|S
ARTICLES
Published on Web 02/03/2005

Polyynes as a Model for Carbyne: Synthesis, Physical Properties, and Nonlinear Optical Response

Sara Eisler,[†] Aaron D. Slepkov,[‡] Erin Elliott,[†] Thanh Luu,[†] Robert McDonald,[†] Frank A. Hegmann,*[,‡] and Rik R. Tykwinski*[,†]

Contribution from the Department of Chemistry, University of Alberta, Edmonton, Alberta T6G 2G2, Canada, and the Department of Physics, University of Alberta, Edmonton, Alberta T6G 2J1, Canada

Received September 9, 2004; E-mail: hegmann@phys.ualberta.ca; rik.tykwinski@ualberta.ca

Abstract: With the Fritsch−Buttenberg−Wiechell rearrangement as a primary synthetic route, a series of conjugated, triisopropylsilyl end-capped polyynes containing 2−10 acetylene units has been assembled. In a few steps, significant quantities of the polyynes are made available, which allow for a thorough analysis of their structural, physical, and optical properties. Molecules in the series have been characterized in detail using ^{13}C NMR spectroscopy, differential scanning calorimetry, mass spectrometry, and, for four derivatives including octayne **6**, X-ray crystallography. UV−vis spectroscopy of the polyynes **1**−**7** shows a consistent lowering of the HOMO−LUMO gap (E_g) as a function of the number of acetylene units (n), fitting a power-law relationship of $E_g \sim n^{-0.379\pm0.002}$. The third-order nonlinear optical (NLO) properties of the polyyne series have been examined, and the nonresonant molecular second hyperpolarizabilities (γ) increase as a function of length according to the power-law $\gamma \sim n^{4.28\pm0.13}$. This result exhibits an exponent that is larger than theoretically predicted for polyynes and higher than is observed for polyenes and polyenynes. The combined linear and nonlinear optical results confirm recent theoretical studies that suggest polyynes as model 1-D conjugated systems. On the basis of UV−vis spectroscopic analysis, the effective conjugation length for this series of polyynes is estimated to be ca. $n = 32$, providing insight into characteristics of carbyne.

Introduction

An sp-hybridized carbon allotrope is notably absent from the list of known carbon allotropes that currently includes diamond, graphite, fullerenes, and nanotubes. Cyclic allotropes consisting entirely of sp-hybridized carbon have been the object of intense interest for many years,[1−4] and several of these species have been observed fleetingly.[5,6] Carbyne, the hypothetical linear form of carbon consisting entirely of sp-hybridized carbon atoms,[7−9] has, to date, presented a significant synthetic challenge, and the allure of this elusive allotrope has stimulated a resurged interest in end-capped sp-hybridized carbon chains (Chart 1).[10] Polyynes are the oligomeric cousins of carbyne, and it is expected that the properties of carbyne might be predicted by extrapolating trends observed in the spectroscopic data for a structurally related series of polyynes.[11] sp-Hybridized carbon oligomers are also interesting in their own right because of their unique electronic, optical, and physical properties.

Chart 1

carbyne

Series 2 n = 2,4,6,8,10

Series 1 n = 3–8

Series 3 n = 3–6,8,10

Series 4 n = 2–6,8,10,12

[†] Department of Chemistry.
[‡] Department of Physics.

(1) Faust, R. *Angew. Chem., Int. Ed.* **1998**, *37*, 2825−2828.
(2) Clemmer, D. E.; Jarrold, M. F. *J. Am. Chem. Soc.* **1995**, *117*, 8841−8850.
(3) von Helden, G.; Gotts, N. G.; Bowers, M. T. *Nature* **1993**, *363*, 60−63.
(4) Goroff, N. S. *Acc. Chem. Res.* **1996**, *29*, 77−83.
(5) Diederich, F.; Rubin, Y.; Chapman, O.; Goroff, N. S. *Helv. Chim. Acta* **1994**, *77*, 1441−1457 and references therein.
(6) Tobe, Y.; Umeda, R.; Iwasa, N.; Sonoda, M. *Chem.−Eur. J.* **2003**, *9*, 5549−5559 and references therein.
(7) Smith, P. P. K.; Buseck, P. R. *Science* **1982**, *216*, 984−986.
(8) Kudryavtsev, Y. P.; Evsyukov, S.; Guseva, M.; Babaev, V.; Khvostov, V. In *Chemistry and Physics of Carbon*; Thrower, P. A., Ed.; Marcel Dekker: New York, 1997; Vol. 25, pp 1−69.
(9) Cataldo, F. *Polym. Int.* **1997**, *44*, 191−200.
(10) Lagow, R. J.; Kampa, J. J.; Wei, H.-C.; Battle, S. L.; Genge, J. W.; Laude, D. A.; Harper, C. J.; Bau, R.; Stevens, R. C.; Haw, J. F.; Munson, E. *Science* **1995**, *267*, 362−367.
(11) Martin, R. E.; Diederich, F. *Angew. Chem., Int. Ed.* **1999**, *38*, 1350−1377.

10.1021/ja044526l CCC: $30.25 **© 2005 American Chemical Society**

The past half century is rich in polyyne syntheses. Early synthetic efforts resulted in the formation of hydrogen,[12−14] alkyl,[15−18] aryl,[18−20] and trialkylsilyl[13] end-capped derivatives.[21] In many cases, polyynes consisting of between 2 and 12 acetylene units could be achieved, but longer derivatives could only be identified by UV−vis and IR spectroscopy because of their kinetic instability. Nonetheless, these earlier efforts afforded a number of impressive molecules, including *t*Bu−(C≡C)$_{12}$−*t*Bu[18] and Et$_3$Si−(C≡C)$_{16}$−SiEt$_3$.[13]

Recent studies of extended polyynes have focused primarily on two goals: (a) more fully exploring polyyne properties using modern methods of analysis and (b) experimenting with a wider range of terminal functionality. Variation of end groups has resulted in the formation of an interesting and diverse group of structures, including iodine,[22] porphyrin,[23] and chalcogen[24] end-capped polyynes. In addition to cyanopolyynes (Chart 1, Series 1)[25] the group of Hirsch has recently reported the synthesis of polyyne chains end-capped by bulky dendrimeric groups (Series 2),[26] culminating in a completely characterized decayne. Metal-capped polyynes have also been extensively studied.[27−30] The work of Gladysz and co-workers has provided the longest metal-capped polyynes to date (Series 3 and 4),[31] including a fully characterized Re end-capped decayne.[31c]

Despite the obvious interest in their formation, there are surprisingly few ways to synthetically assemble polyyne chains, and the most popular methods remain the Cu$^{I/II}$-catalyzed oxidative homocoupling protocols.[32] While these techniques have been successfully used to form extended polyynes, one of the greatest problems remains the inability to produce and isolate significant quantities of the longest compounds, such as C_{16} and C_{20}. As a result, the opportunity to fully explore the properties of polyynes has been greatly restricted.

Chart 2

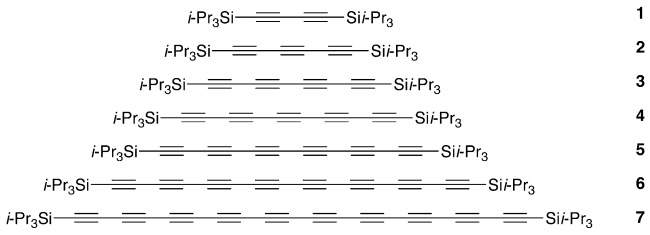

Interest in conjugated polyynes continues to be motivated both by the synthetic challenge, as well as a desire to explore their fundamental properties. In the past several years, the Fritsch−Buttenburg−Wiechell (FBW) rearrangement has emerged as a convenient route to diynes, triynes, and 2-D carbon networks.[33,34] Optimization of this process for the realization of extended polyynes has now been achieved and offers synthetic advantages over traditional methods of polyyne synthesis. First, a variety of techniques are available to form the stable dibromoolefinic precursors and provide numerous routes to extend chain length.[33a] Facile purification of both synthetic intermediates and products is also an important feature of the FBW route, while generally high-yielding steps also provide macroscopic quantities of pure samples. For the current study, a series of triisopropylsilyl (TIPS) end-capped polyynes **1**−**7** has been assembled (Chart 2). The simple, but bulky, TIPS moiety has been incorporated because it provides both solubility and stability. In addition, it does not dramatically alter the electronic makeup of the carbon chains, allowing for an analysis of an essentially pure sp-hybridized carbon system.

Results and Discussion

Dimer **1** and tetramer **3** were synthesized via an oxidative homocoupling reaction,[35] and trimer **2** was synthesized by a FBW rearrangement, as reported.[33a] Diederich has previously reported the synthesis of pentayne **4**, with the central acetylene introduced in the final synthetic step via flash vacuum pyrolysis (FVP).[36] To avoid the necessity of assembling an FVP apparatus, the FBW approach was used as an alternative for the synthesis of pentayne **4**.

Protiodesilylation of differentially protected enediyne **8**[37] provided terminal acetylene **9** (Scheme 1). Subsequent deprotonation with LDA and condensation with triisopropylsilylpro-

(12) Kloster-Jensen, E. *Angew. Chem., Int. Ed. Engl.* **1972**, *11*, 438−439.
(13) Eastmond, R.; Johnson, T. R.; Walton, D. R. M. *Tetrahedron* **1972**, *28*, 4601−4615.
(14) For recent examples, see: (a) Tsuji, M.; Kuboyama, S.; Matsuzaki, T.; Tsuji, T. *Carbon* **2003**, *41*, 2141−2148. (b) Cataldo, F. *Carbon* **2004**, *42*, 129−142.
(15) Cook, C. L.; Jones, E. R. H.; Whiting, M. C. *J. Chem. Soc.* **1952**, 2883−2891.
(16) Bohlmann, F. *Chem. Ber.* **1953**, *86*, 657−667.
(17) Jones, E. R. H.; Lee, H. H.; Whiting, M. C. *J. Chem. Soc.* **1960**, 3483−3489.
(18) Johnson, T. R.; Walton, D. R. M. *Tetrahedron* **1972**, *28*, 5221−5236.
(19) Armitage, J. B.; Entwhistle, N.; Jones, E. R. H.; Whiting, M. C. *J. Chem. Soc.* **1954**, 147−154.
(20) Nakagawa, M.; Akiyama, S.; Nakasuji, K.; Nishimoto, K. *Tetrahedron* **1971**, *27*, 5401−5418.
(21) For an excellent review of this earlier work, see: Hopf, H. *Classics in Hydrocarbon Synthesis*; Wiley-VCH: Weinheim, Germany, 2000; Chapter 8.
(22) Gao, K.; Goroff, N. S. *J. Am. Chem. Soc.* **2000**, *122*, 9320−9321.
(23) Nakamura, K.; Fujimoto, T.; Takara, S.; Sugiura, K.; Miyasaka, H.; Ishii, T.; Yamashita, M.; Sakata, Y. *Chem. Lett.* **2003**, *32*, 694−695.
(24) (a) Werz, D. B.; Gleiter, R. *J. Org. Chem.* **2003**, *68*, 9400−9405. (b) Werz, D. B.; Gleiter, R.; Rominger, F. *Organometallics* **2003**, *22*, 843−849.
(25) Schermann, G.; Grösser, T.; Hampel, F.; Hirsch, A. *Chem.−Eur. J.* **1997**, *3*, 1105−1112.
(26) Gibtner, T.; Hampel, F.; Gisselbrecht, J. P.; Hirsch, A. *Chem.−Eur. J.* **2002**, *8*, 408−432.
(27) Bunz, U. H. F. *Angew. Chem., Int. Ed. Engl.* **1996**, *35*, 969−971.
(28) (a) Bruce, M. I.; Low, P. J. *Adv. Organomet. Chem.* **2004**, *50*, 179−444. (b) Bruce, M. I. *Coord. Chem. Rev.* **1997**, *166*, 91−119.
(29) Long, N. J.; Williams, C. K. *Angew. Chem., Int. Ed.* **2003**, *42*, 2586−2617.
(30) For selected recent examples, see: (a) Antonova, A. B.; Bruce, M. I.; Ellis, B. G.; Gaudio, M.; Humphrey, P. A.; Jevric, M.; Melino, G.; Nicholson, B. K.; Perkins, G. J.; Skelton, B. W.; Stapleton, B.; White, A. H.; Zaitseva, N. N. *Chem. Commun.* **2004**, 960−961. (b) Yam, V. W. W.; Wong, K. M. C.; Zhu, N. Y. *Angew. Chem., Int. Ed.* **2003**, *42*, 1400−1403. (c) Xu, G. L.; Zou, G.; Ni, Y. H.; DeRosa, M. C.; Crutchley, R. J.; Ren, T. *J. Am. Chem. Soc.* **2003**, *125*, 10057−10065. (d) Lu, W.; Xiang, H.-F.; Zhu, N.; Che, C.-M. *Organometallics* **2002**, *21*, 2343−2346. (e) Sakurai, A.; Akita, M.; Moro-oka, Y. *Organometallics* **1999**, *18*, 3241−3244. (f) Akita, M.; Chung, M.-C.; Sakurai, A.; Sugimoto, S.; Terada, M. *Organometallics* **1997**, *16*, 4882−4888.
(31) (a) Mohr, W.; Stahl, J.; Hampel, F.; Gladysz, J. A. *Chem.−Eur. J.* **2003**, *9*, 3324−3340. (b) Stahl, J.; Bohling, J. C.; Bauer, E. B.; Peters, T. B.; Mohr, W.; Martin-Alvarez, J. M.; Hampel, F.; Gladysz, J. A. *Angew. Chem., Int. Ed.* **2002**, *41*, 1872−1876. (c) Dembinski, R.; Bartik, T.; Bartik, B.; Jaeger, M.; Gladysz, J. A. *J. Am. Chem. Soc.* **2000**, *122*, 810−822. (d) Bartik, B.; Dembinski, R.; Bartik, T.; Arif, A. M.; Gladysz, J. A. *New J. Chem.* **1997**, *21*, 739−750. (e) Bartik, T.; Bartik, B.; Brady, M.; Dembinski, R.; Gladysz, J. A. *Angew. Chem., Int. Ed. Engl.* **1996**, *35*, 414−417.
(32) Siemsen, P.; Livingston, R. C.; Diederich, F. *Angew. Chem., Int. Ed.* **2000**, *39*, 2633−2657.
(33) (a) Eisler, S.; Chahal, N.; McDonald, R.; Tykwinski, R. R. *Chem.−Eur. J.* **2003**, *9*, 2542−2550. (b) Shi Shun, A. L. K.; Chernick, E. T.; Eisler, S.; Tykwinski, R. R. *J. Org. Chem.* **2003**, *68*, 1339−1347. (c) Shi Shun, A. L. K.; Tykwinski, R. R. *J. Org. Chem.* **2003**, *68*, 6810−6813. (d) Chernick, E. T.; Eisler, S.; Tykwinski, R. R. *Tetrahedron Lett.* **2001**, *42*, 8575−8578. (e) Eisler, S.; Tykwinski, R. R. *J. Am. Chem. Soc.* **2000**, *122*, 10736−10737.
(34) A carbene-based route has also been developed for alkyne synthesis; see ref 6 and Tobe, Y.; Iwasa, N.; Umeda, R.; Sonoda, M. *Tetrahedron Lett.* **2001**, *42*, 5485−5488.
(35) Hlavaty, J.; Kavan, J.; Kubista, J. *Carbon* **2002**, *40*, 345−349.
(36) Rubin, Y.; Lin, S. S.; Knobler, C. B.; Anthony, J.; Boldi, A. M.; Diederich, F. *J. Am. Chem. Soc.* **1991**, *113*, 6943−6949.
(37) Anthony, J.; Boldi, A. M.; Rubin, Y.; Hobi, M.; Gramlich, V.; Knobler, C. B.; Seiler, P.; Diederich, F. *Helv. Chim. Acta* **1995**, *78*, 13−45.

Scheme 1. Synthesis of Pentayne **4**

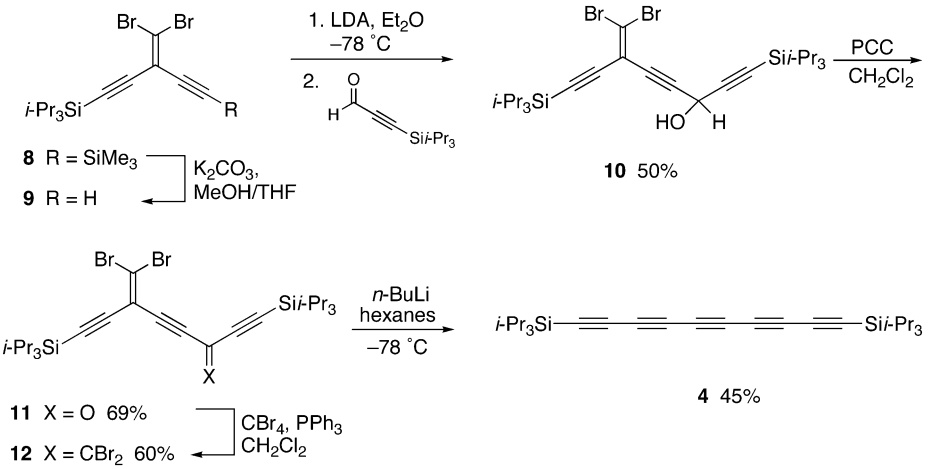

Scheme 2. Synthesis of Hexayne **5**

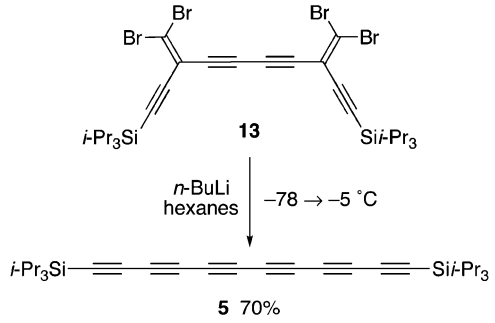

Scheme 3. Synthesis of Octayne **6**

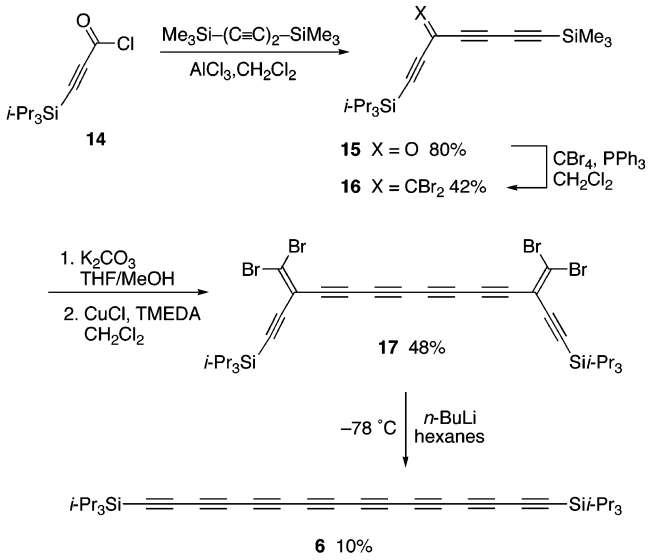

pargyl aldehyde gave **10** as a stable yellow oil in 50% yield. The alcohol was easily oxidized to ketone **11** using PCC, and a Corey−Fuchs[38] reaction gave tetrabromide **12** as a stable solid. The final step, a 2-fold rearrangement, proceeded smoothly using a standard procedure of slow addition of 2.4 equiv of BuLi to a solution of **12** in hexanes at −78 °C.[39] Aqueous workup and chromatographic removal of baseline material gave pentayne **4** in 45% yield as a white crystalline solid that is stable indefinitely when kept under refrigeration.

As previously reported,[33a] the synthesis of hexayne **5** was straightforward from dimer **13** via a dual rearrangement (Scheme 2). Hexayne **5** was isolated as a pale yellow solid that is also stable indefinitely under refrigeration.

Friedel−Crafts acylation has been a powerful method of directly forming conjugated ketones,[40] and the reaction of acid chloride **14** with 1,4-bis(trimethylsilyl)-1,3-butadiyne produced ketone **15** in an excellent yield of 80% (Scheme 3). Reaction of **15** under Corey−Fuchs conditions gave dibromide **16** as a stable yellow oil. Containing eight of the necessary 16 conjugated carbons, **16** was then dimerized under Hay conditions[41] to form the polyyne precursor **17**, which is a surprisingly stable solid under ambient conditions. The modest yield of this step was likely due to competitive cross-coupling reaction between the terminal acetylene and the vinyl bromide in the presence of $Cu^{I/II}$ (Castro−Stephens coupling).[42] Rearrangement was induced with BuLi to produce octayne **6**,[39] which, following chromatographic purification, can be readily recrystallized from hexanes to give an orange/yellow solid that is stable indefinitely at low temperature. While the yield of this 2-fold reaction was lower than that in the case of the penta- and hexayne, an overall yield of 10% was obtained, representing a 33% yield for each rearrangement event.

As demonstrated, the polyynes **4**−**6** are assembled fairly easily, and even the octayne **6** can be constructed in a few days in fairly large quantities. The longer the polyyne, however, the more elaborate the synthesis. This reality is reflected in the formation of the final compound in the series, **7**, only the third fully characterized decayne known to date (Scheme 4).

The initial stages of the synthesis of decayne **7** were analogous to the formation of pentayne **4**. The lithium acetylide was formed from **9** with LDA and reacted with trimethylsilylpropargyl aldehyde to afford alcohol **18** in 46% yield as a stable

(38) (a) Ramirez, F.; Desai, N. B.; McKelvie, N. *J. Am. Chem. Soc.* **1962**, *84*, 1745−1747. (b) Corey, E. J.; Fuchs, P. L. *Tetrahedron Lett.* **1972**, 3769−3772. (c) Posner, G.; Loomis, G. L.; Sawaya, H. S. *Tetrahedron Lett.* **1975**, 1373−1376.

(39) The point at which quenching was initiated was essential to the success of the rearrangement. If quenched too soon, byproducts resulting from protonation of the lithiated intermediates are formed and greatly complicate purification because of similar retention times on chromatographic supports. TLC analysis was therefore required during the warming stage to ensure complete rearrangement. The reaction mixture was consequently allowed to warm up to ∼−5 °C to ensure complete rearrangement. See Supporting Information for complete experimental details.

(40) Walton, D. R. M.; Waugh, F. *J. Organomet. Chem.* **1972**, *37*, 45−56.

(41) Hay, A. S. *J. Org. Chem.* **1962**, *27*, 3320−3321.

(42) Stephens, R. D.; Castro, C. E. *J. Org. Chem.* **1963**, *28*, 3313−3315.

Scheme 4. Synthesis of Octabromide **21**

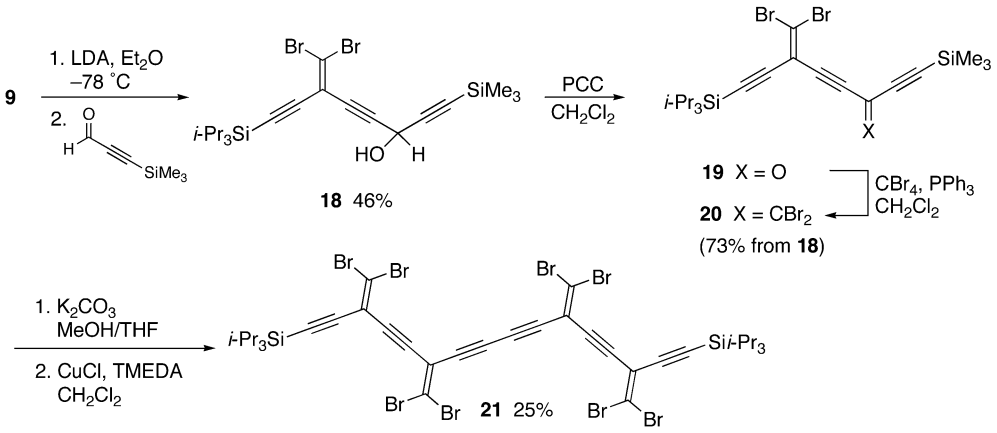

Scheme 5. Synthesis of Decayne **7**

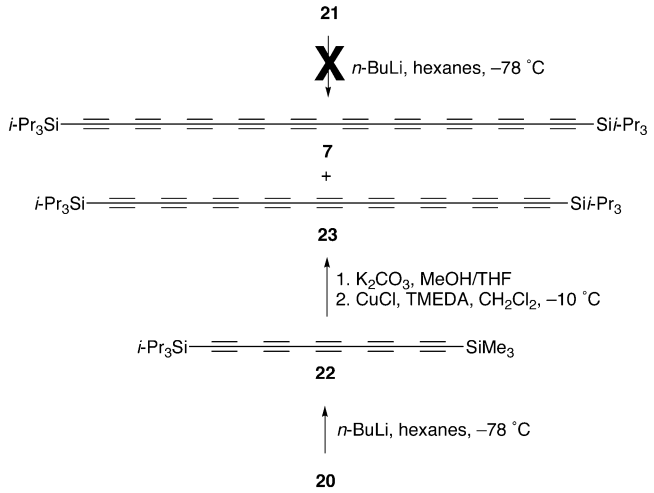

yellow oil. Following oxidation with PCC, the crude product **19** was passed through a short silica gel column and carried on directly to the Corey−Fuchs reaction without further purification. Overall, this process gave an excellent yield of the differentially protected tetrabromide **20** and put into place the 10-carbon section of decayne **7**. Tetrabromide **20** was selectively deprotected, and the central carbon−carbon bond of **21** was introduced using standard Hay conditions to give octabromide **21** as a stable oil that slowly solidified over time under refrigeration.

Several attempts were then made to effect a quadruple rearrangement **21** → **7** (Scheme 5). The standard reaction conditions developed for **4**−**6** were, however, disappointingly ineffective and apparently too harsh for the extended π-rich intermediates formed during the course of the reaction. For example, addition of BuLi to a solution of **21** at −78 °C and warming to −20 °C resulted in incomplete rearrangement, and none of the desired product decayne **7** could be detected. Warming of the reaction to higher temperature in hopes of encouraging complete rearrangement of all alkylidene centers, however, produced only intractable black solids. It was unclear, at this point, whether the inability to effect formation of **7** resulted from an inherent instability of the product (**7**), or from a failing of the FBW approach. Thus, an alternative, more traditional approach was explored. The 10-carbon segment **20** was converted to the differentially protected pentayne **22**. Rewardingly, this step went very well, and no byproducts resulting from incomplete rearrangement were observed by TLC. The less bulky TMS group is clearly less effective at stabilizing a pentayne core than the TIPS moiety, and pentayne **22** was found to be kinetically much less stable than its structural cousin **4**. Attempted purification of pentayne **22** by column chromatography on silica gel led to partial removal of the TMS moiety, and, therefore, the crude product **22** was simply passed through a plug of silica with hexanes to remove baseline material and then carried on directly to complete protiodesilylation. As expected, the resulting terminal acetylene from **22** was quite unstable, and it was therefore carried directly on to an oxidative-coupling reaction. Initially, homocoupling of this 10-carbon segment was attempted in CH_2Cl_2 at room temperature with an excess of CuCl and TMEDA, the standard Hay conditions. TLC analysis indicated the reaction was complete almost immediately, and following workup and chromatographic purification, one product was apparently isolated. Analysis of this product by UV−vis spectroscopy, however, showed the presence of an unexpected and problematic byproduct. Polyynes have very distinctive and well-defined UV−vis absorption spectra (vide infra), and it became clear upon analysis of the reaction mixture of **22** → **7** that, in addition to the presence of the decayne **7**, nonayne **23** had also been formed in ca. 10% yield; the two products were inseparable.[43] It was subsequently determined that the formation of the nonayne can be almost completely suppressed by lowering the temperature of the homocoupling reaction. Thus, oxidative homocoupling of deprotected **22** at −10 °C, followed by column chromatography (silica gel, hexanes) and passage of a hexanes solution of the product **7** in through a plug of alumina gave the bright orange decayne **7** in a yield of 30% from **20**. While **7** shows limited stability when exposed to chromatography supports (silica gel and alumina) or ambient light and temperatures for extended periods of time, it can be stored indefinitely when kept cold (−4 °C).

Differential Scanning Calorimetry. The thermal stability of polyynes **1**−**7** was investigated using differential scanning calorimetry (DSC).[44] Polyynes **1**−**5** each show an endothermic phase transition corresponding to a reproducible melting point. Crystalline diyne **1** shows three endotherms, the final one a

(43) During the course of our study, Hirsch and co-workers reported a similar observation; see ref 26. To the best of our knowledge, these are the only two known examples of an apparent loss of C2 during a Hay coupling reaction. Cleavage of single bonds in polyynes has, however, been reported for other metals (e.g., Zr and Ti). See: Rosenthal, U.; Pellny, P. M.; Kirchbauer, F. G.; Burlakov, V. V. *Acc. Chem. Res.* **2000**, *33*, 119−129.

(44) DSC traces of compounds **1**−**7** can be found in the Supporting Information.

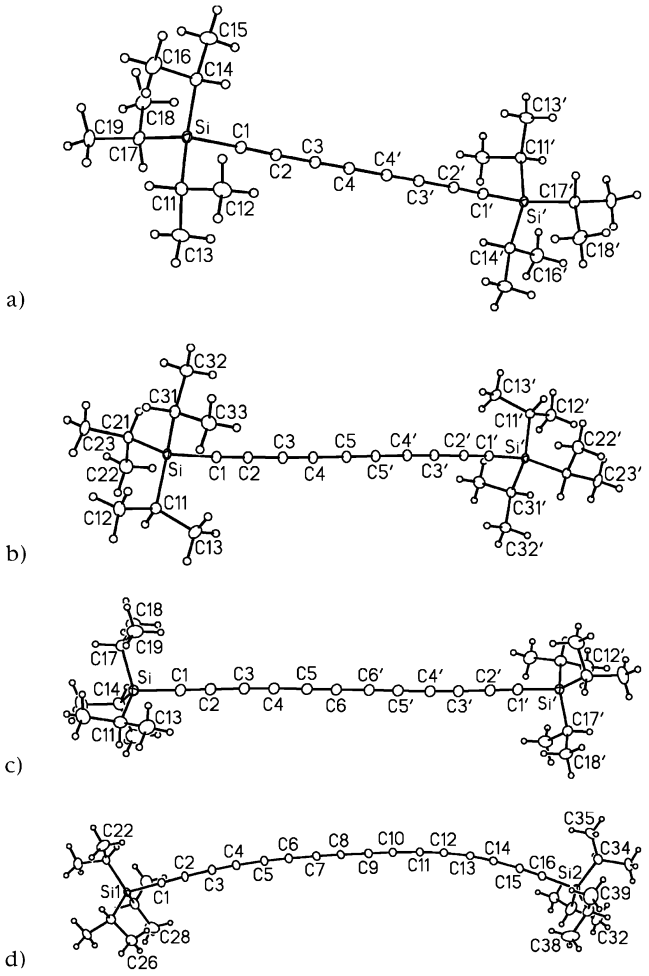

Figure 1. ORTEP representations for (a) tetrayne **3**, (b) pentayne **4**, (c) hexayne **5**, and (d) octayne **6** (all shown at 20% probability).

melting point at 100 °C.[45] Triyne **2** shows an endotherm with an onset temperature T_o = 149 °C, with a maximum T_{max} = 154 °C, and the sample remains stable as a neat liquid through the temperature range measured (up to 250 °C). For tetrayne **3** (T_o = 77 °C, T_{max} = 83 °C), pentayne **4** (T_o = 105 °C, T_{max} = 110 °C), and hexayne **5** (T_o = 67 °C, T_{max} = 77 °C), the initial endotherm is followed by a broad exothermic transition centered at 251, 204, and 177 °C, respectively. By contrast, octayne **6** shows a sharp, symmetrical exotherm, centered at 132 °C and spanning only 9 °C, characteristic of a topochemical polymerization reaction.[46,47] This observation correlates well with the solid-state molecular alignment determined by X-ray crystallographic analysis (vide infra). Decayne **7** also shows no melting point with only a broad exotherm observed at 123 °C as a result of decomposition or nonregioselective polymerization.

Crystallographic Analysis. Crystals suitable for X-ray crystallographic analysis were obtained for compounds **3**−**6**, grown by the slow diffusion of MeOH into a CH_2Cl_2/hexane solution at 4 °C. In the solid state, the structures of tetrayne **3**, pentayne **4**, and hexayne **5** are centrosymmetic and essentially linear (Figure 1a−c). Of the four structures, octayne **6**, only the second structurally characterized octayne to date,[48] has the most unusual shape (Figure 1d). Each individual acetylene unit bears only a slight deviation from linearity with an average C≡C−X (X = C or Si) bond angle of 176.9°, presumably due to crystal packing effects. Overall, however, the cumulative effect of these deviations results in a rather dramatic curvature in an unsymmetrical bow shape. The shape of **6** most closely resembles that of a platinum end-capped hexayne reported by Gladysz and co-workers (Chart 1, Series 4, n = 6),[31a] which shows a symmetric bow conformation with a slightly lower average C≡C−X bend of 174.6°.

Within this series of polyynes, a reduction in the degree of bond-length alternation is predicted as one proceeds to longer and longer derivatives.[47] Disappointingly, however, a comparison of bond length as a function of conjugation length provided no distinct trends indicative of reduced bond length alternation. All bond lengths are unremarkable.[49]

The solid-state packing for compounds **3**−**6** provides a means of correlating solid-state (in)stability and intermolecular orientation. The crystal packing diagram of tetrayne **3** (Figure 2) shows the molecules are aligned in a parallel manner, as seen looking down both the crystallographic *a*- and *b*-axis. Although molecules are offset in a manner for which a topochemical polymerization process might be possible, the interatomic distance between reacting carbons for a 1,4-, 1,6-, and 1,8-polymerization ranges from 5.3 to 6.9 Å, and is thus too great in all cases.[46,47] This renders an interchain polymerization reaction impossible and corroborates the thermal stability observed for **3** in the DSC analysis.

The solid-state packing of the pentayne **4**, when viewed down the crystallographic *a*-axis (Figure 3a), shows alternating rows of molecules oriented at ca. 120° with respect to each other, with the closest interatomic sp−sp carbon contacts separated by a distance of 4 Å. Conversely, when viewed along the crystallographic *b*-axis, parallel alignment of the molecules is observed. Within each row, however, the interatomic closest contacts at a distance of 6.9 and 7.7 Å are too great for either a 1,4- or 1,6-polymerization reaction to occur, respectively.

The solid-state herringbone structure of hexayne **5** (Figure 4) is similar to that for pentayne **4**. The molecules are aligned in rows along the crystallographic *a*-axis, although the closest contacts of neighboring molecules within a row are still greater than 5 Å and thus too far separated for a topochemical reaction (Figure 4a). When viewed down the *c*-axis, molecular stacking is offset by approximately 145° (Figure 4b).

Thus, for compounds **3**−**5**, the solid-state arrangement of neighboring molecules is such that topochemical polymerization, in a specific manner, is unlikely. This factor corroborates the stability of these solids at room temperature, as well as the DSC results that clearly indicate a defined melting point for each of these compounds.

This situation is different for octayne **6**. The crystal packing for octayne **6** highlights the notable bend of the molecule as viewed down the *a*-axis (Figure 5a) and also shows that molecules clearly pack in an alternating fashion to accommodate the bulky TIPS groups. There is alignment of the gently curving

(45) The thermal behavior of α,ω-bis(trialkylsilyl)butadiynes has been extensively studied. See: Carré, F.; Devylder, N.; Dutremez, S. G.; Guérin, C.; Henner, B. J. L.; Jolivet, A.; Tomberli, W.; Dahan, F. *Organometallics* **2003**, *22*, 2014−2033.
(46) Enkelmann, V. *Chem. Mater.* **1994**, *6*, 1337−1340.
(47) Szafert, S.; Gladysz, J. A. *Chem. Rev.* **2003**, *103*, 4175−4205.
(48) For the other octayne structure, see ref 31a. For an excellent summary of the crystallographic and solid-state properties of polyynes, see ref 47. A preliminary account of the structure of hexayne **5** can be found in ref 47.
(49) A tabular summary of bond lengths for **3**−**6** is provided in the Supporting Information.

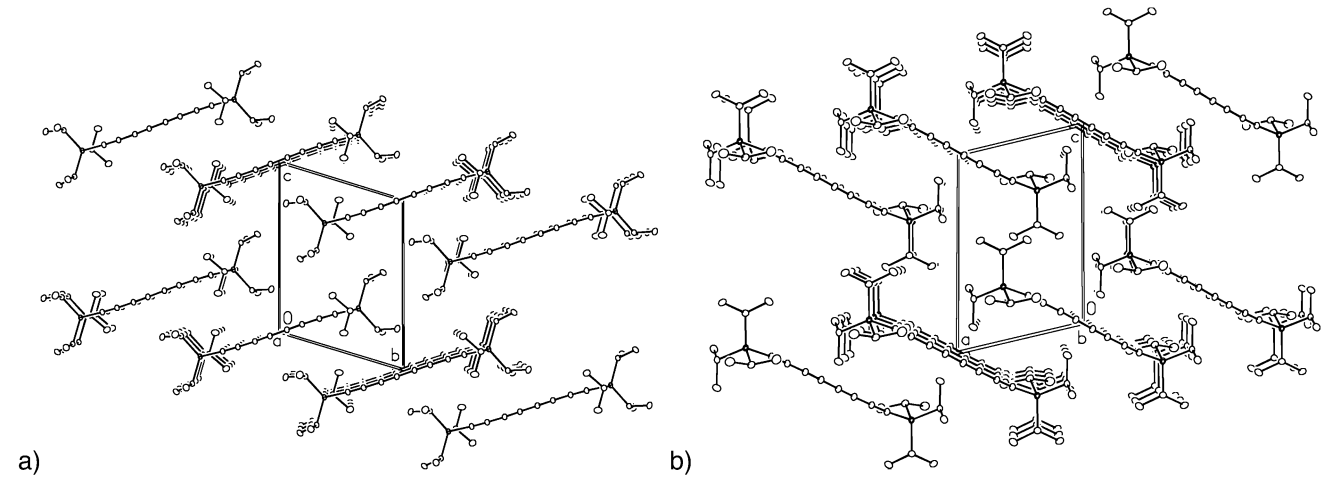

Figure 2. Crystal packing diagram of tetrayne **3**, as viewed along the (a) crystallographic *a*-axis and (b) crystallographic *b*-axis (hydrogen atoms omitted for clarity).

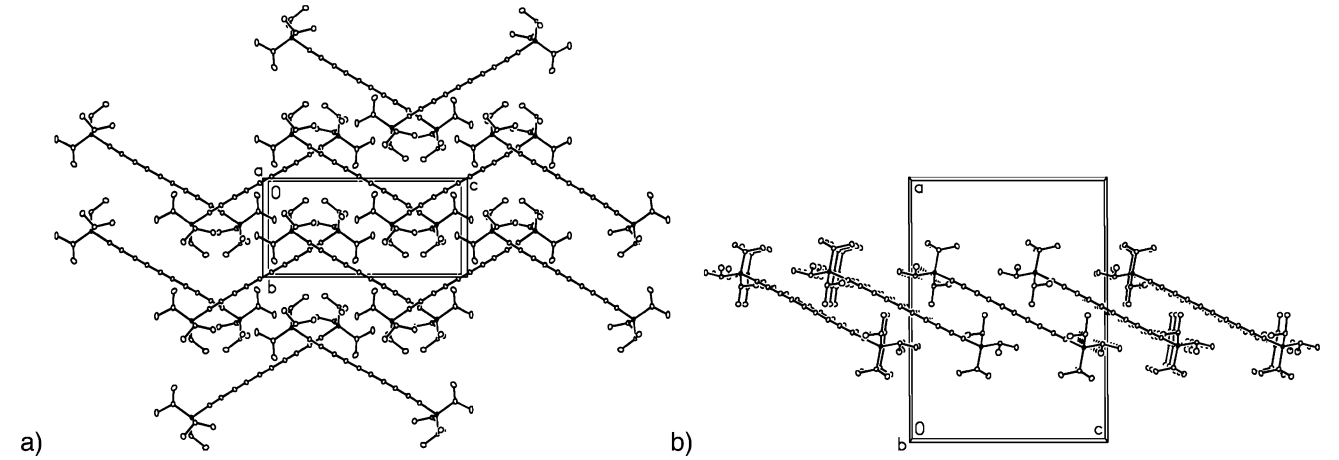

Figure 3. Crystal packing diagram of pentayne **4**, as viewed along the (a) crystallographic *a*-axis and (b) crystallographic *b*-axis (hydrogen atoms omitted for clarity).

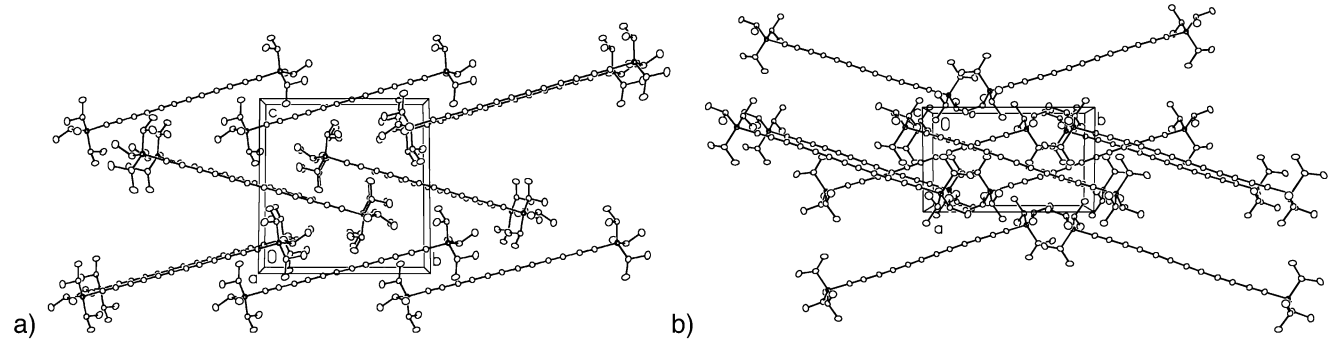

Figure 4. Crystal packing diagram of hexayne **5**, as viewed along the (a) crystallographic *a*-axis and (b) crystallographic *c*-axis (hydrogen atoms omitted for clarity).

structures down the *a*-axis that affords a number of close contacts between neighboring molecules in the range of 3.5−4 Å, which are suitable for topochemical polymerization.[46,47] Furthermore, the packing orientation is well within the range expected to afford 1,6-polymerization.[46,47] Nonetheless, octayne **6** remains free from polymerization at room temperature, presumably due to a significant kinetic barrier to this solid-state reaction. As described above, however, DSC analysis of a crystalline sample of **6** supports the notion that thermal polymerization can be initiated at temperatures greater than 130 °C.

^{13}C NMR Spectroscopy. The distinctive ^{13}C NMR spectra of polyynes **1**−**7** were very useful in confirming the structure of the compounds in this series, and each individual carbon resonance was well resolved for all molecules. Figure 6 shows an expansion of the ^{13}C NMR spectrum for each molecule containing the signals of the sp-hybridized carbons. There are two distinct areas of interest. Region 1 contains the two lower field resonances, which are the carbons for the acetylene unit closest to the triisopropylsilyl groups, C1 and C2, confirmed by ^{13}C labeling.[50] Region 2 contains resonances for all of the internal sp-hybridized carbons. The separation of the C1 and

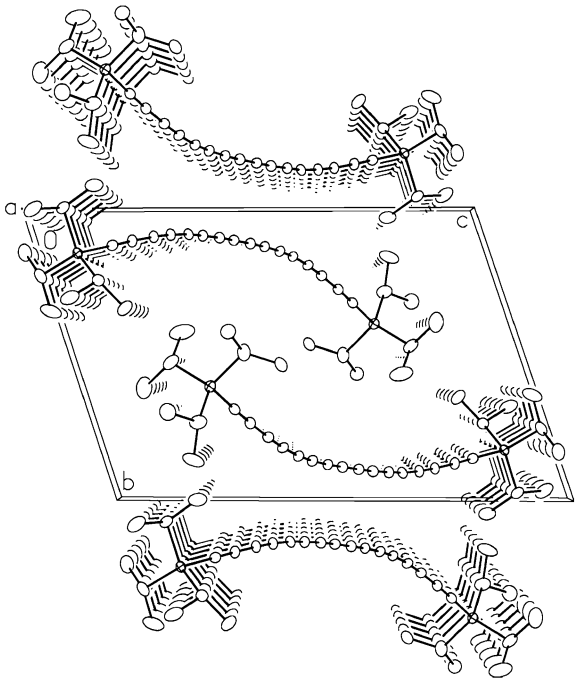

Figure 5. Crystal packing diagram of **6** viewed down the crystallographic *a*-axis (hydrogen atoms omitted for clarity).

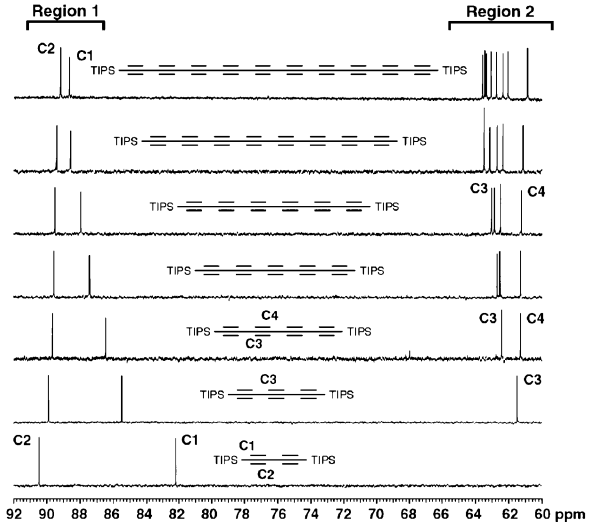

Figure 6. ^{13}C NMR spectra of polyynes **1**−**7** (CD_2Cl_2, 125 MHz).

C2 resonances from those of the internal carbons is not unexpected, as they are the most chemically distinct because of their proximity to the TIPS moiety. Intuition might suggest that C1 and C2 would be the least affected by an increase in chain length, as the TIPS groups remain a consistent feature in each molecule. As can be seen, however, the chemical shifts of C1 and C2 converge upon moving from the diyne to the decayne. The most dramatic change is that of C1, which is shifted downfield from 82.2 ppm for diyne **1** to 88.8 ppm for decayne **7**.

Region 2 of the NMR spectra contains the resonances of the internal carbons, observed between 60 and 64 ppm. At a certain length, saturation should occur and these internal resonances will cease to be resolved but will instead merge into one signal. At C_{20}, however, saturation has yet to be reached, and all internal

(50) See Supporting Information for details and discussion.

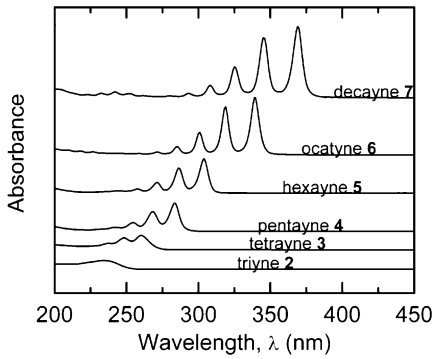

Figure 7. UV−vis absorption spectra for the *i*-$Pr_3Si-(C{\equiv}C)_n-Si$*i*-Pr_3 series, as measured in hexanes (spectra have been shifted vertically for display).

resonances are well resolved at 125 MHz. For triyne **2**, the signal for the internal sp carbon, C3, is observed at 61.5 ppm. An analogous signal appears at nearly the same chemical shift for each polyyne regardless of chain length; for example, in the spectrum of decayne **7** it is found at 61.0 ppm. As one progresses to longer derivatives, an interesting trend is observed, as has been reported for other polyyne series.[26,31c] There is a consistent appearance of new signals in the narrow range of 62−63 ppm and apparently converging at an asymptotic limit for TIPS(C≡C)$_\infty$TIPS that would be characteristic of carbyne. While it was tempting to assign the signal consistently found at ca. 61 ppm to C3 for each molecule and downfield signals to the internal carbons of the progressively longer alkyne chains, preliminary ^{13}C labeling studies have definitively shown that the analysis is more intricate than this. Using a straightforward synthetic sequence,[50] we selectively labeled tetrayne **3** with ^{13}C at carbon C4. The ^{13}C NMR spectrum for this molecule clearly shows the labeled C4 resonance at δ 61.3, while the unlabeled C3 resonance is found at δ 62.4. While it has been, to date, synthetically more challenging to selectively introduce a ^{13}C label to a single position in the longer polyynes, it has been possible to label hexayne **5** with ^{13}C distributed at C3 and C4.[50] Analysis of the ^{13}C NMR spectrum of this molecule shows signals resulting from the labeled carbons C3 at δ 63.0 and C4 at δ 61.2. Thus, for hexayne **5** as well, the resonance at 61.2 ppm is not assignable to C3, but arises from C4. As a result of this analysis, one might tentatively assign the most *upfield* signal observed in region 2 of the ^{13}C NMR spectra of **2**−**7** to C4 of the polyyne chain, and the most *downfield* resonance in region 2 as that of C3. Clearly, however, this suggestion begets additional labeling studies that are beyond the scope of the current report, studies which are, however, underway.

Linear Optical Properties. Tremendous insight into the electronic landscape of polyynes may be achieved by UV−vis spectroscopic characterization. The UV−vis spectra of the TIPS polyynes are presented in Figure 7, with the most relevant data listed in Table 1.[51] In contrast to most other conjugated organic molecules, the high-energy region of the UV spectra (220−270 nm) of the longest polyynes, octayne **6** and decayne **7**, is nearly transparent. This rare characteristic could allow for interesting optical applications of polyynes within this window

(51) A preliminary account of these results has been reported. See: Slepkov, A. D.; Hegmann, F. A.; Eisler, S.; Elliott, E.; Tykwinski, R. R. *J. Chem. Phys.* **2004**, *120*, 6807−6810. For a discussion of the electronic properties of cross-conjugated enynes such as **12**, **13**, and **17**, see: Zhao, Y.; McDonald, R.; Tykwinski, R. R. *J. Org. Chem.* **2002**, *67*, 2805−2812.

Table 1. UV−vis and Nonlinear Optical Characterization of *i*-$Pr_3Si-(C\equiv C)_n-Si$*i*-Pr_3

compd	*n*	λ_{max} (nm)[a]	E_g (cm^{-1})[a]	ϵ_{max} (L mol^{-1} cm^{-1})[a]	γ (10^{-36} esu)[b]
1	2	<210	>47 600	−	2.75 ± 0.28
2	3	234	42 700	92 700	7.02 ± 0.70
3	4	260	38 500	157 000	12.5 ± 2.1
4	5	284	35 200	293 000	35.3 ± 1.2
5	6	304	32 900	359 000	64.5 ± 2.9
6	8	339	29 500	603 000	238 ± 47
7	10	369	27 100	753 000	646 ± 27

[a] As measured in hexanes. [b] As measured at 800 nm in THF; all values are an average of at least three independent measurements.

of transparency. The vibronic structure is clearly visible, appearing as a series of narrow absorption peaks with steadily increasing intensity toward the visible region. The highest-wavelength absorption peak (λ_{max}) for each polyyne oligomer reflects a transition from the lowest energy vibrational level in the ground state to the lowest energy vibrational level in the excited state. There is a corresponding increase in the molar absorptivity (ϵ) as the chain length increases, and the TIPS end-capped systems show some of the highest molar absorptivity values measured for polyynes, with octayne **6** at $\epsilon = 603\,000$ L mol^{-1} cm^{-1} and decayne **7** at $\epsilon = 753\,000$ L mol^{-1} cm^{-1}. A comparison of ϵ-values at λ_{max} for **7** to that of other known decaynes highlights the dramatic dependence of the oscillator strength on the nature of the end group: a rhenium end-capped decayne (Chart 1, Series 3)[31c] shows $\epsilon = 190\,000$ L mol^{-1} cm^{-1}, a dendrimer-terminated decayne (Chart 1, Series 2)[26] shows $\epsilon = 605\,000$ L mol^{-1} cm^{-1}, while a decayne terminated with *t*-Bu groups[17] shows $\epsilon = 850\,000$ L mol^{-1} cm^{-1}.

A red-shift in λ_{max} is clearly visible as the length of the carbon rods is increased, indicating a decrease in the HOMO → LUMO energy gap (Figure 7). At a particular chain length, however, saturation of this effect is expected, where λ_{max} would reach a minimum and constant value (λ_{sat}), representing the effective conjugation length for this series of polyyne oligomers. At this point, λ_{sat} would also be an estimate of the HOMO → LUMO band gap of carbyne. Considering electron correlation effects, the empirical power-law $E_g = 1/\lambda_{max} \sim n^{-x}$ describes the relationship between E_g, λ_{max}, and n (where E_g is the energy of the HOMO → LUMO gap in cm^{-1}).[52,53] This relationship is depicted in Figure 8 and shows a consistent power-law decrease in E_g through at least C_{20} that can be fit quite precisely to $E_g \sim n^{-0.379\pm0.002}$. While this behavior is different from that reported by Gladysz and co-workers, who report $E_g \sim n^{-1}$ for rhenium end-capped polyynes (Chart 1, Series 3),[31c] it is close to the well-established "Lewis−Calvin Law" of $E_g \sim n^{-0.5}$ observed for many polyenic materials.[54−56] Since the power-law decrease in E_g depicted in Figure 8 includes all of the oligomers, saturation of the HOMO−LUMO gap has clearly not yet been initiated in this series.

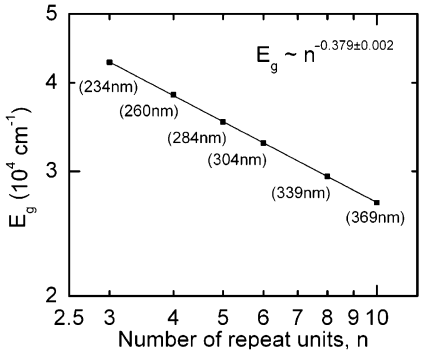

Figure 8. Power-law plot of the lowest absorption energy and the number of repeat units, *n*, in the *i*-$Pr_3Si-(C\equiv C)_n-Si$*i*-Pr_3 series, with corresponding λ_{max} values given in parentheses. The solid line represents the line-of-best-fit to the data with $E_g \sim n^{-0.379\pm0.002}$, where $E_g = 1/\lambda_{max}$.[56]

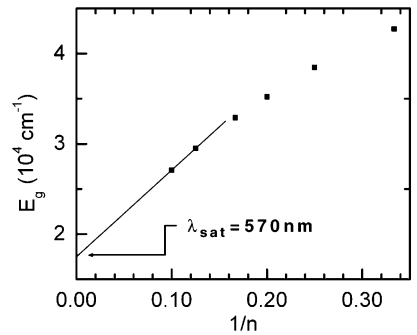

Figure 9. Plot of the HOMO−LUMO band-gap energy E_g versus 1/*n* for the TIPS end-capped polyynes. An absorption wavelength of $\lambda_{sat} = 570$ nm is extrapolated as a prediction for $n = \infty$.

Because increasing polyyne length should eventually lead to an asymptotic λ_{max} value representative of carbyne (λ_{sat}), it is interesting to extrapolate toward the electronic absorption properties of this infinite length oligomer. Following the analysis of Gladysz and others,[26,31c] a plot of E_g versus 1/*n* is used to estimate the λ_{max} absorption value of an infinite polyyne chain in this series (Figure 9), and a value of $\lambda_{sat} = 570$ nm is predicted by extrapolation to the *y*-intercept. This estimate is considerably higher than that of 400 nm predicted by semiempirical calculations.[57] It is, however, nearly identical to that of 569 nm[26] and 565 nm[31c] predicted for Series 2 and 3 (Chart 1), respectively.

With an estimated value for $\lambda_{max} = 570$ nm for carbyne (i.e., λ_{sat} from Figure 9), it is now possible to estimate the effective conjugation length for TIPS end-capped polyynes and to provide a tentative answer to the question: "How long is carbyne?" Thus, depicting the power-law shown in Figure 8 in terms of the number of repeat units, *n*,[56] yields:

$$n = (\lambda_{max}/154\ \text{nm})^{2.638} \qquad (1)$$

where λ_{max} is in nanometers. Assuming that the trend in Figure 8 trend is maintained until rapid saturation occurs and that $\lambda_{max} = \lambda_{sat} = 570$ nm is the HOMO−LUMO limit at $n = \infty$, a value of $n \approx 32$ is obtained for carbyne from eq 1. Thus, 64 consecutive sp-hybridized carbons would represent the effective conjugated length for this series of polyynes and provides the best experimental estimate of the minimum conjugation length of carbyne.

(52) Bubeck, C. In *Electronic Materials: The Oligomer Approach*; Müllen, K., Wegner, G., Eds.; Wiley-VCH: Weinheim, Germany, 1998, Chapter 8.
(53) Luo, Y.; Norman, P.; Ruud, K.; Agren, H. *Chem. Phys. Lett.* **1998**, *285*, 160−163.
(54) Lewis, G. N.; Calvin, M. *Chem. Rev.* **1939**, *25*, 273−328.
(55) Mathy, A.; Ueberhofen, K.; Schenk, R.; Gregorius, H.; Garay, R.; Müllen, K.; Bubeck, C. *Phys. Rev. B* **1996**, *53*, 4367−4376.
(56) The full form of the power-law is $E_g = an^{-x}$, which shows a best fit to the parameters of $a = 64\,900$ cm^{-1} and $x = 0.379$, as presented in Figure 8. Thus, transforming this equation in terms of length and wavelength (in nanometers) gives $\lambda_{max} = (1/E_g)$, $(1/x) = 2.638$, and $(1/a) = 154$ nm. A comparison of the relationship shown in Figure 8 to that of Lewis−Calvin is provided as Supporting Information (as are R^2 values).
(57) Scemama, A.; Chaquin, P.; Gazeau, M. C.; Bénilan, Y. *Chem. Phys. Lett.* **2002**, *361*, 520−524.

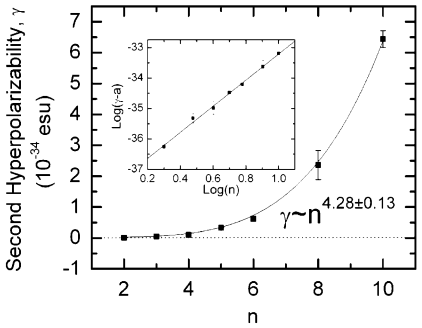

Figure 10. Polyyne molecular second hyperpolarizability, γ, as a function of the number of repeat units, *n*. The solid lines are a fit of the form $\gamma = a + bn^c$, where *a* is an offset due to a contribution from the TIPS moiety to the overall response. Inset: log−log plot of the same data with the coefficient *a* subtracted, yielding a power-law exponent (slope of the solid line) of $c = 4.28 \pm 0.13$ for the polyyne series **1**−**7**.

Nonlinear Optical Properties. The molecular second hyperpolarizabilities, γ, of TIPS polyynes have been determined using a differential optical Kerr effect (DOKE) detection setup.[51] In this time-resolved pump−probe technique, amplified, 100-fs, 800-nm laser pulses at a 1 kHz repetition rate are utilized for nonresonant γ measurements of polyyne samples **1**−**7** in THF solutions. A nonlinearity for THF of $\gamma_{THF} = 5.2 \times 10^{-37}$ esu, measured by the DOKE setup, was used as a reference for the samples.[58,59]

Polyynes **1**−**7** all display an ultrafast electronic second hyperpolarizability (γ) that follows the autocorrelation of the laser pulses with negligible two-photon absorption. As seen in Table 1 and Figure 10, the polyynes yield relatively small nonlinearities at short chain lengths. The increase in molecular second hyperpolarizability with increased chain length is, however, rapid. By the stage of the decamer **7**, the nonlinearity is quite sizable: $\gamma = (6.5 \pm 0.3) \times 10^{-34}$ esu. By way of comparison, β-carotene, a polyene with 22 consecutive sp^2-hybridized carbons, shows a γ-value of $(7.9 \pm 0.8) \times 10^{-34}$ esu, as measured in THF with the DOKE setup. The similarity between γ-values for **7** and β-carotene contrasts theoretical studies on oligomers of analogous length that predict substantially smaller values for polyyne nonlinearities compared to those for polyenes.[60,61]

For a given series of conjugated oligomers, γ-values are known to increase superlinearly as a function of length.[52,62,63] For oligomers shorter than the effective conjugation length, theoretical models invariably predict a power-law dependence of $\gamma \sim n^c \sim L^{c'}$, where *L* is the length of the molecule, *n* is the number of repeat units, and *c* or *c*′ is the power-law exponent.[64,65] Both theoretically and experimentally, the exponent *c* remains the most commonly used figure of merit for the comparison of third-order optical nonlinearities among different oligomer series.[52] Whereas a constant exponent *c* is expected for small- to medium-length oligomers, as the chain length approaches the effective conjugation length, the onset of saturation will manifest itself as a decreasing *c* value.[66] Once saturation is reached, increasing the length of the oligomer does not increase the extent of conjugation, and γ will vary linearly with oligomer length (i.e., $c = 1$). Various values of *c* have been theoretically predicted for organic oligomers, depending on the theoretical model used. In studies that consider π-conjugated systems in general, predictions range from $c = 5$ for both the "free electron in a box" and the one-electron Hückel models, to $c = 3.2$ for more complex approximations that account for electron-correlation effects.[52,67] Most computational models yield an exponent around $c = 4$.[52] Theoretical studies specifically addressing polyyne γ-values predict exponents from $c = 1.26$ to 3.3.[61,68,69] While it is difficult to make a direct comparison between the various predictions, one important trend does emerge: all studies predict power-law exponents for polyynes that are smaller than those for polyenes.[61,67,68] Empirically this is not unexpected, given the more polarizable electrons of the sp^2-hybridized framework of polyenes versus the sp-hybridization of polyynes.

A fit of γ-values for polyynes **1**−**7** follows the power-law function $\gamma = a + bn^c$, where *a* represents a small offset due to the nonlinear response of the TIPS moieties (Figure 10) and the exponent is $c = 4.28 \pm 0.13$. Consistent with the linear absorption data discussed above, this trend is continuous through the series **1**−**7**, showing no sign of the onset of saturation. To the best of our knowledge, this is the largest exponent observed for a series of conjugated oligomers.[70] Whereas judgments based on absolute γ-values obtained by different research groups are problematic, power-law exponents are much less sensitive to the experimental method employed and therefore allow for comparisons between different systems. Thus, for example, the third-order nonlinear optical (NLO) response of polytriacetylenes, the closest structural relative to polyynes, shows power-law behavior with a reported exponent of $c = 2.5$.[71] Furthermore, oligo(1,4-phenyleneethynylene)s also show an exponent of $c = 2.5$,[72] and power-law exponents ranging from $c = 2.3$ to 3.6 have been reported for polyenes.[66,67,73]

Experimentally, the magnitude of the power-law exponent observed here for polyynes **1**−**7** is surprisingly high in comparison to that for other conjugated materials. Several factors may account for this observation. The major component to the molecular second hyperpolarizability in organic molecules arises from electron delocalization along the conjugated backbone

(58) Slepkov, A. D.; Hegmann, F. A.; Zhao, Y. M.; Tykwinski, R. R.; Kamada, K. *J. Chem. Phys.* **2002**, *116*, 3834−3840.
(59) Slepkov, A. D. M. Sc. Thesis, University of Alberta, Edmonton, Alberta, Canada, 2002.
(60) Perpète, E. A.; Champagne, B.; Andre, J. M.; Kirtman, B. *J. Mol. Struct. Theochem.* **1998**, *425*, 115−122.
(61) Nalwa, H. S.; Mukai, J.; Kakuta, A. *J. Phys. Chem.* **1995**, *99*, 10766−10774.
(62) Brédas, J.-L.; Adant, C.; Tackx, P.; Persoons, A.; Pierce, B. M. *Chem. Rev.* **1994**, *94*, 243−278.
(63) Gubler, U.; Bosshard, C. *Adv. Polym. Sci.* **2002**, *158*, 123−191.
(64) For an alternative approach and analysis, see: Schulz, M.; Tretiak, S.; Chernyak, V.; Mukamel, S. *J. Am. Chem. Soc.* **2000**, *122*, 452−459.
(65) Whereas there is some debate as to the interchangeability of *L* and *n* as a universal parameter, for polyynes, the two parameters scale identically.
(66) Samuel, I. D. W.; Ledoux, I.; Dhenaut, C.; Zyss, J.; Fox, H. H.; Schrock, R. R.; Silbey, R. J. *Science* **1994**, *265*, 1070−1072.
(67) Nalwa, H. S. In *Nonlinear Optics of Organic Molecules and Polymers*; Nalwa, H. S., Miyata, S., Eds.; CRC Press: Boca Raton, FL, 1997; Chapters 9 and 11.
(68) Buma, W. J.; Fanti, M.; Zerbetto, F. *Chem. Phys. Lett.* **1999**, *313*, 426−430.
(69) Archibong, E. F.; Thakkar, A. J. *J. Chem. Phys.* **1993**, *98*, 8324−8329.
(70) With the possible exception of oligorylenes, for which a power-law behavior with an exponent of $c = 5.6$ was estimated. See: Rumi, M.; Zerbi, G.; Müllen, K.; Müller, G.; Rehahn, M. *J. Chem. Phys.* **1997**, *106*, 24−34.
(71) (a) Martin, R. E.; Gubler, U.; Boudon, C.; Gramlich, V.; Bosshard, C.; Gisselbrecht, J. P.; Günter, P.; Gross, M.; Diederich, F. *Chem.−Eur. J.* **1997**, *3*, 1505−1512. (b) Gubler, U.; Bosshard, C.; Günter, P.; Balakina, M. Y.; Cornil, J.; Brédas, J.-L.; Martin, R. E.; Diederich, F. *Opt. Lett.* **1999**, *24*, 1599−1601.
(72) Meier, H.; Ickenroth, D.; Stalmach, U.; Koynov, K.; Bahtiar, A.; Bubeck, C. *Eur. J. Org. Chem.* **2001**, 4431−4443.
(73) Craig, G. S. W.; Cohen, R. E.; Schrock, R. R.; Silbey, R. J.; Puccetti, G.; Ledoux, I.; Zyss, J. *J. Am. Chem. Soc.* **1993**, *115*, 860−867.

(longitudinal hyperpolarizability).[52,53,67] Linear polyynes undergo minimal conformational disorder in solution and maintain orbital overlap along the molecular axis. Unlike polyenic compounds, where rotation about single bonds can interrupt conjugation, the linear conjugated framework of polyynes maintains orbital overlap under bond rotation.[74] Thus, polyynes better reflect the idealized geometries (linear and rigid) and display larger solution-state γ-values.[75] Furthermore, in comparison to an sp^2-hybridized oligomer with an essentially planar π-electron system, the longitudinal hyperpolarizability of a polyyne (with a cylindrical π-system) would be less dependent on solution-state orientation with respect to the electric field of the incident light source, which would also enhance γ-values.

The experimentally determined power-law exponent of $c = 4.28$ for **1**−**7** is also significantly higher than that predicted theoretically for polyynes ($c = 1.26$ to 3.3, vide supra).[61,68,69] This may be due, in part, to simplified models and geometries that have been used in some studies, and more sophisticated computational models may yield better agreement with the experimental results determined here for **1**−**7**. For example, the effect of electron correlation has been identified as more significant for the molecular hyperpolarizabilities of polyynes than other conjugated oligomers, and the effect increases with the length of the polyyne chain.[76] Thus, the role of electron correlation effects in polyynes may hold the key to bridging the experimental and theoretical third-order NLO results.[76−78] In addition to electron correlation effects, frequency dispersion and changes in geometry also impact calculated NLO properties of linear π-systems.[78] In fact, a recent report demonstrates that the MP2/6-31G* method can provide geometrical data in good agreement with experiments.[79] Unfortunately, γ-values have not yet been computed with these improved geometries. Nonetheless, the fact remains that not only do polyynes **1**−**7** display a surprisingly rapid increase in second hyperpolarizability with increasing chain length, but also the power-law exponent describing this increase is larger for polyynes than for any polyene system previously investigated.

The keys to explaining the intriguing linear and nonlinear optical properties of polyynes may lie in how closely these sp-hybridized carbon rods model an ideal 1-D conjugated system. Comparing the hyperpolarizabilities of polyynes **1**−**7** with predictions on the upper bound γ-values of 1-D π-conjugated systems proves interesting. Recently, Kuzyk[80] has proposed the theoretical upper limit for γ in linear conjugated organic systems as:

$$\gamma_{xxxx} < 4e^4\hbar^4 m^{-2} N^2 E_g^{-5} \qquad (2)$$

where e is the electron charge, $\hbar$ is Planck's constant, m is the electron mass, N is the number of electrons, and E_g is the first excited-state transition energy. Substituting the power-law relationship of $E_g \sim n^{-0.379}$ into eq 2 and assuming that the number of delocalized electrons scales linearly with the number of multiple bonds (i.e., $N \propto n$) gives $\gamma_{xxxx} \sim n^{3.90}$ as the predicted upper bound scaling for γ for polyynes **1**−**7**. This value is quite close to our measured value of $\gamma \sim n^{4.28}$, and to date, polyynes are the first 1-D system to experimentally demonstrate power-law behavior approaching this theoretical limit.[80,81]

It has also been recently shown by Luo et al.[53] that random phase approximation (RPA) calculations for conjugated materials predict power-law increases in both the longitudinal nonlinearities γ_{xxxx} and the HOMO−LUMO energy gap E_g with increasing chain length. Interestingly, having modeled a range of conjugated oligomers (polyacenes, polyphenylenes, *cis*- and *trans*-polyenes, etc.), Luo et al. report universal behavior that is independent of the system modeled, with $E_g \sim L^{-0.38\pm0.02}$ and $\gamma \sim L^{4.2\pm0.1}$ (where L is the oligomer length). Because polyyne length scales directly with the number of repeat units (n), the values of $E_g \sim L^{-0.379\pm0.002}$ and $\gamma \sim L^{4.28\pm0.13}$ determined experimentally in the present study are in excellent agreement with the RPA calculations, further indicating that polyynes behave optically as ideal 1-D conjugated materials.

Conclusions

The synthesis of triisopropylsilyl end-capped polyynes with up to 20 sp-hybridized carbons has been developed and provides sufficient quantities of pure material such that an extensive study of their physical and optical properties could be accomplished. Spectroscopic analyses of this series provide numerous trends in the characteristics of these molecules as a function of length, and an estimated conjugation length for carbyne of 32 acetylene units is predicted on the basis of UV−vis analysis. A comparison of the present experimental results to recent theoretical predictions describing both the linear and nonlinear optical characteristics for polyynes strongly supports the fact that polyynes most closely model the behavior expected for true 1-D conjugated systems.

Experimental Section

X-ray Crystal Data for Tetrayne 3: $C_{26}H_{42}Si_2$, formula weight = 410.78, triclinic space group $P\bar{1}$ (No. 2), $Z = 1$, $a = 7.2615(6)$ Å, $b = 8.7028(7)$ Å, $c = 11.4850(9)$ Å, $\alpha = 104.8780(13)°$, $\beta = 100.6479(15)°$, $\gamma = 98.4852(14)°$, $V = 674.70(9)$ Å^3. $T = -80$ °C, final $R_1(F) = 0.0379$, $wR_2(F^2) = 0.1022$ for 127 variables and 2717 unique reflections with $F_o^2 \geq -3\sigma(F_o^2)$ (2474 observations [$F_o^2 \geq 2\sigma(F_o^2)$]), GOF = 1.042.

X-ray Crystal Data for Pentayne 4: $C_{28}H_{42}Si_2$, formula weight = 434.80, monoclinic space group $C2/c$ (No. 15), $Z = 4$, $a = 21.699(3)$ Å, $b = 7.8425(11)$ Å, $c = 16.242(2)$ Å, $\beta = 90.184(3)°$, $V = 2764.0(7)$ Å^3. $T = -80$ °C, final $R_1(F) = 0.0420$, $wR_2(F^2) = 0.1161$ for 136 variables and 2833 unique reflections with $F_o^2 \geq -3\sigma(F_o^2)$ (2414 observations [$F_o^2 \geq 2\sigma(F_o^2)$]), GOF = 1.050.

X-ray Crystal Data for Hexayne 5: $C_{30}H_{42}Si_2$, formula weight = 458.82, monoclinic space group $P2_1/c$ (No. 14), $Z = 2$, $a = 8.2757(6)$ Å, $b = 13.4444(11)$ Å, $c = 13.9444(11)$ Å, $\beta = 97.7225(16)°$, $V = 1537.4(2)$ Å^3. $T = -80$ °C, final $R_1(F) = 0.0402$, $wR_2(F^2) = 0.1067$ for 145 variables and 3156 unique reflections with $F_o^2 \geq -3\sigma(F_o^2)$ (2353 observations [$F_o^2 \geq 2\sigma(F_o^2)$]), GOF = 1.029.

(74) Ledoux, I.; Samuel, I. D. W.; Zyss, J.; Yaliraki, S. N.; Schattenmann, F. J.; Schrock, R. R.; Silbey, R. J. *Chem. Phys.* **1999**, *245*, 1−16.
(75) While the optimal geometry of an alkyne is linear, distortion can occur. For a discussion, see: Krebs, A.; Wilke, J. *Top. Curr. Chem.* **1983**, *109*, 189−233.
(76) Toto, J. L.; Toto, T. T.; Demelo, C. P. *Chem. Phys. Lett.* **1995**, *245*, 660−664.
(77) Torrent-Sucarrat, M.; Sola, M.; Duran, M.; Luis, J. M.; Kirtman, B. *J. Chem. Phys.* **2003**, *118*, 711−718.
(78) Kirtman, B.; Champagne, B. *Int. Rev. Phys. Chem.* **1997**, *16*, 389−420.
(79) Poulsen, T. D.; Mikkelsen, K. V.; Fripiat, J. G.; Jacquemin, D.; Champagne, B. *J. Chem. Phys.* **2001**, *114*, 5917−5922.
(80) (a) Kuzyk, M. G. *Phys. Rev. Lett.* **2000**, *85*, 1218−1221. (b) Kuzyk, M. G. *Phys. Rev. Lett.* **2003**, *90*, 039902. (c) Kuzyk, M. G. *Opt. Lett.* **2000**, *25*, 1183−1185. (d) Kuzyk, M. G. *Opt. Lett.* **2003**, *28*, 135−135.
(81) Contributions to delocalization resulting from the silyl groups are expected to be small. See: Trætteberg, M.; Bakken, P.; Liebman, J. F.; Hulce, M. *J. Mol. Struct.* **1995**, *346*, 101−109.

X-ray Crystal Data for Octayne 6: $C_{34}H_{42}Si_2$, formula weight = 506.86, triclinic space group $P\bar{1}$ (No. 2), $Z = 2$, $a = 7.6441(14)$ Å, $b = 12.485(2)$ Å, $c = 18.300(3)$ Å, $\alpha = 70.701(4)°$, $\beta = 82.758(4)°$, $\gamma = 80.500(4)°$, $V = 1620.9(5)$ Å^3. $T = -80$ °C, final $R_1(F) = 0.0714$, $wR_2(F^2) = 0.1673$ for 325 variables and 6146 unique reflections with $F_o^2 \geq -3\sigma(F_o^2)$ (2637 observations [$F_o^2 \geq 2\sigma(F_o^2)$]), GOF = 0.877.

General Procedure for Alkyne Rearrangements. Unless noted in the individual procedures below, a 0.010−0.016 M solution of the dibromoolefin in hexanes under nitrogen was cooled to −78 °C, and 1.1−1.2 equiv of *n*-BuLi per dibromoolefin moiety was slowly added over a period of ca. 2 min. Reactions were allowed to warm to approximately −10 to −5 °C over a period of 0.5−1 h. The reactions were quenched at ca. −5 °C with an aqueous NH_4Cl solution (10 mL). Diethyl ether was added (20 mL), the organic layer was separated, washed with aqueous NH_4Cl solution (2 × 20 mL), and dried ($MgSO_4$), and the solvent was removed in vacuo. Full details are provided as Supporting Information.

1,4-Bis(triisopropylsilyl)-1,3-butadiyne (1): mp 98−100 °C; R_f = 0.84 (hexanes); UV−vis (hexanes) λ_{max} (ϵ) 208 (48 000) nm; IR (CH_2Cl_2, cast) 2945, 2866, 2061, 1463 cm^{-1}; ^{1}H NMR (500 MHz, CD_2Cl_2) δ 1.09 (s, 42H); ^{13}C NMR (125 MHz, CD_2Cl_2) δ 90.4, 82.2, 18.8, 11.8. EI MS *m*/*z* 362.3 (M$^+$, 38), 319.2 ([M − *i*-Pr]$^+$, 100); EI HRMS *m*/*z* calcd. for $C_{22}H_{42}Si_2$ (M$^+$): 362.2825; found: 362.2818. Compound **1** has been reported previously.[35]

1,6-Bis(triisopropylsilyl)-1,3,5-hexatriyne (2): mp 140 °C; R_f = 0.8 (hexanes); UV−vis (hexanes) λ_{max} (ϵ) 234 (92 700) nm; IR (CH_2Cl_2, cast) 2945, 2866, 2154, 1462 cm^{-1}; ^{1}H NMR (500 MHz, CD_2Cl_2) δ 1.09 (s, 42H); ^{13}C NMR (125 MHz, CD_2Cl_2) δ 89.9, 85.5, 61.5, 18.7, 11.6; EI MS *m*/*z* 386.3 (M$^+$, 34), 343.2 ([M − *i*-Pr]$^+$, 100); EI HRMS *m*/*z* calcd. for $C_{24}H_{42}Si_2$ (M$^+$): 386.2825; found: 386.2819. Compound **2** has been reported previously.[33a]

1,8-Bis(triisopropylsilyl)-1,3,5,7-octatetrayne (3): mp 72−75 °C; R_f = 0.87 (hexanes); UV−vis (hexanes) λ_{max} (ϵ) 260 (157 000), 248 (130 000), 239 (84 000) nm; IR (CH_2Cl_2, cast) 2944, 2866, 2042, 1462 cm^{-1}; ^{1}H NMR (500 MHz, CD_2Cl_2) δ 1.09 (s, 42H); ^{13}C NMR (125 MHz, CD_2Cl_2) δ 89.7, 86.5, 62.4, 61.3, 18.7, 11.7; EI MS *m*/*z* 410.3 (M$^+$, 33), 367.2 ([M − *i*-Pr]$^+$, 100); EI HRMS *m*/*z* calcd. for $C_{26}H_{42}Si_2$ (M$^+$): 410.2825; found: 410.2825. Compound **3** has been reported previously.[35]

1,10-Bis(triisopropylsilyl)-1,3,5,7,9-decapentayne (4): mp 104−105 °C; R_f = 0.79 (hexanes); UV−vis (hexanes) λ_{max} (ϵ) 284 (293 000), 268 (205 000), 255 (89 800), 242 (42 000) nm; IR (CH_2Cl_2, cast) 2943, 2178, 2030, 1461 cm^{-1}; ^{1}H NMR (500 MHz, CD_2Cl_2) δ 1.09 (s, 42H); ^{13}C NMR (125 MHz, CD_2Cl_2) δ 89.5, 87.4, 62.7, 62.5, 61.3, 18.7, 11.7; EI MS *m*/*z* 434.3 (M$^+$, 37), 391.2 ([M − *i*-Pr]$^+$, 100); EI HRMS *m*/*z* calcd. for $C_{28}H_{42}Si_2$ (M$^+$): 434.2825; found: 434.2822. Compound **4** has been previously synthesized by other means.[6,36]

1,12-Bis(triisopropylsilyl)-1,3,5,7,9,11-dodecahexayne (5): mp 78−80 °C; R_f = 0.87 (hexanes); UV−vis (hexanes) λ_{max} (ϵ) 304 (359 000), 286 (262 000), 271 (112 000), 258 (43 100), 245 (24 200) nm; IR (CH_2Cl_2, cast) 2866, 2158, 2030, 1462 cm^{-1}; ^{1}H NMR (500 MHz, CD_2Cl_2) δ 1.09 (s, 42H); ^{13}C NMR (125 MHz, CD_2Cl_2) δ 89.5, 87.9, 63.0, 62.8, 62.5, 61.2, 18.7, 11.8; EI MS *m*/*z* 458.3 (M$^+$, 42), 415.2 ([M − *i*-Pr]$^+$, 100); EI HRMS *m*/*z* calcd. for $C_{30}H_{42}Si_2$ (M$^+$): 458.2825; found: 458.2834. Compound **5** has been reported previously.[33a]

1,16-Bis(triisopropylsilyl)-1,3,5,7,9,11,13,15-hexadecaoctayne (6): mp 93−95 °C; R_f = 0.95 (hexanes); UV−vis (hexanes) λ_{max} (ϵ) 339 (603 000), 319 (505 000), 301 (237 000), 285 (89 200), 271 (31 700) nm; IR (CH_2Cl_2, cast) 2943, 2119, 2021, 1958, 1461 cm^{-1}; ^{1}H NMR (500 MHz, CD_2Cl_2) δ 1.08 (s, 42H); ^{13}C NMR (125 MHz, CD_2Cl_2) δ 89.4, 88.5, 63.4, 63.4, 63.1, 62.6, 62.3, 61.1, 18.7, 11.7; ESI MS (nitromethane, AgOTf added) *m*/*z* 674 ([M + Ag$^+$ + solvent], 30), 1121 ([2M + Ag] $^+$, 100).

1,20-Bis(triisopropylsilyl)-1,3,5,7,9,11,13,15,17,19-einacosadecayne (7): mp 105−113 °C (dec); R_f = 0.88 (hexanes); UV−vis (hexanes) λ_{max} (ϵ) 369 (753 000), 345 (633 000), 325 (326 000), 308 (131 000), 293 (47 300) nm; IR (CH_2Cl_2, cast) 2923, 2072, 1462 cm^{-1}; ^{1}H NMR (500 MHz, CD_2Cl_2) δ 1.08 (s, 42H); ^{13}C NMR (125 MHz, CD_2Cl_2) δ 89.3, 88.8, 63.8, 63.6, 63.5, 63.2, 62.9, 62.5, 62.2, 61.0, 18.7, 11.7; MS (MALDI, retinoic acid matrix) 555.3 (MH$^+$).

Acknowledgment. This work was supported by the National Sciences and Engineering Research Council of Canada (NSERC), iCORE, ASRA, CFI, IIPP, CIPI, and the University of Alberta. Petro-Canada is gratefully acknowledged for a Young Innovator Award (R.R.T.), NSERC for a postgraduate scholarship (A.D.S.) and an undergraduate research fellowship (E.E.), Alberta Ingenuity for a graduate scholarship (A.D.S.), and the University of Alberta for a Province of Alberta Research Fellowship (S.E.). We thank Dr. M. J. Ferguson for the X-ray crystallographic analysis of **4**.

Supporting Information Available: General procedures, instrumental methods, experimental and spectroscopic data for all new compounds, DSC traces for compounds **1**−**7**, experimental and spectral details for ^{13}C labeling studies, a Lewis−Calvin plot for comparison to Figure 8, and crystallographic data for compounds **3**−**6** (PDF, CIF). This material is available free of charge via the Internet at http://pubs.acs.org.

JA044526L